ELSEVIER

Journal of Biomechanics 37 (2004) 1313–1320

JOURNAL OF BIOMECHANICS

www.elsevier.com/locate/jbiomech
www.JBiomech.com

A three-dimensional digital image correlation technique for strain measurements in microstructures

E. Verhulp, B. van Rietbergen*, R. Huiskes

Department of Biomedical Engineering, Eindhoven University of Technology, Room WH 4.128, Den Dolech 2, 5600 MB Eindhoven, The Netherlands

Accepted 28 December 2003

Abstract

A three-dimensional digital image correlation technique is presented for strain measurements in open-cell structures such as trabecular bone. The technique uses high-resolution computed tomography images for displacement measurements in the solid structure. In order to determine the local strain-state within single trabeculae, a tetrahedronization method is used to fill the solid structure with tetrahedrae. Displacements are calculated at the nodes of the tetrahedrae. The displacement data is subsequently converted to a deformation tensor in each of the tetrahedral element centers with a least-squares estimation method. Because the trabeculae are represented by a mesh, it is possible to deform this mesh according to the deformation tensor and, at the same time, visualize the calculated local strain in the deformed mesh with a finite element post-processing tool. In this way, the deformation of a single trabecula from an aluminum foam sample was determined and validated with rendered images of the three-dimensional sample. A precision analysis showed that a rigid translation or rotation does not affect the accuracy. Typical values for the standard deviation in the displacement and strain components are 2.0 μm and 0.01, respectively. Presently, the precision limits the technique to strain measurements beyond the yield strain.

Keywords: Strain measurements; Trabecular bone; Image correlation; Computed tomography

1. Introduction

The mechanical properties of trabecular bone are intensively studied for clinical applications, as in age-related fractures and bone and joint replacements. The majority of the experimental, analytical and numerical studies published focused on the macroscopic, or continuum-level, properties of this cellular material. Certain continuum-level properties, however, are largely determined by conditions at the local (tissue) level. For example, a local increase in stress and strain in trabecular bone can start biological (e.g. remodeling) and mechanical (e.g. microdamage) processes, which affect the structure as a whole. Hence, for a better understanding of the mechanobiology of trabecular bone both the tissue properties and the local stress and strain states are needed.

Although optical methods have been used to measure displacements of markers on individual trabeculae near the surface of deformed samples (Odgaard and Linde, 1991), no methods have been reported that enable detailed measurements of local deformation at the level of bone trabeculae, not even for excised bone samples. As an alternative approach, micro-finite element (μFE) analyses have been used to calculate local strains in finite element models that represent the actual trabecular architecture (Hollister et al., 1994; van Rietbergen et al., 1995, 1999; Niebur et al., 2000). Such models, however, calculate strains as a function of bone loading, architecture and assumed tissue material properties, and hence do not provide direct measurements of strains in bone tissue.

Several years ago a digital image correlation technique was developed that enables strain measurement by correlating the position of pixels in images of undeformed and deformed objects. Although this technique has been applied to measure local deformations from two-dimensional cortical bone images (Nicolella et al., 2001), only continuum-level strain distributions have

*Corresponding author. Tel.: +31-40-2474773; fax: +31-40-2447355.
E-mail address: b.v.rietbergen@tue.nl (B.van Rietbergen).

0021-9290/$ - see front matter © 2004 Elsevier Ltd. All rights reserved.
doi:10.1016/j.jbiomech.2003.12.036

been reported from two- (Bay, 1995) and three-dimensional (Bay et al., 1999) trabecular bone images. Although such measurements provide information about the distribution of the homogenized strains, they do not quantify strains in the bone tissue itself.

In this study a three-dimensional digital image correlation technique is presented that measures local strain in single trabeculae, imaged with micro-Computed Tomography (μCT). A two-dimensional digital image correlation technique (Sutton et al., 1986) was extended to three dimensions and adjusted for strain measurement in porous trabecular bone-like materials. The aim of the study was to determine the precision for local strain measurements of the extended image correlation technique.

2. Materials and methods

2.1. Displacement measurement

The three-dimensional digital image correlation technique presented is based on a two-dimensional technique developed by Sutton et al. (1986). Their optimized image correlation technique maximizes the correlation coefficient R by minimizing the function

$$S = 1 - R = 1 - \frac{\sum_{i,j=1}^{N} a(x_i, y_j) b(x'_i, y'_j)}{\left(\sum_{i,j=1}^{N} a(x_i, y_j)^2 \sum_{i,j=1}^{N} b(x'_i, y'_j)^2\right)^{1/2}}. \quad (1)$$

The $N \times N$ matrices a and b contain a subset of the reference and deformed images, respectively (Fig. 1). Minimizing the function S corresponds to a search for the best position and deformation of the subset a, but now in the deformed image. Linear deformation is used to link a position (x,y) in the reference image with the corresponding position (x',y') in the deformed image,

$$x' - x = u + \frac{\partial u}{\partial x} dx + \frac{\partial u}{\partial y} dy, \quad (2a)$$

$$y' - y = v + \frac{\partial v}{\partial x} dx + \frac{\partial v}{\partial y} dy, \quad (2b)$$

where u and v are the displacement components at the center of subset a in the x and y directions, respectively. This means that, in two dimensions, S is a function of six independent variables denoted by the vector

$$\mathbf{w}_{2D} = \left(u,\ v,\ \frac{\partial u}{\partial x}, \frac{\partial u}{\partial y}, \frac{\partial v}{\partial x}, \frac{\partial v}{\partial y}\right).$$

The image correlation technique was extended to three dimensions for strain measurements based on CT-images. In three dimensions a similar function of 12 variables has to be minimized to find the vector

$$\mathbf{w}_{3D} = \left(u,\ v,\ w,\ \frac{\partial u}{\partial x}, \frac{\partial u}{\partial y}, \frac{\partial u}{\partial z}, \frac{\partial v}{\partial x}, \frac{\partial v}{\partial y}, \frac{\partial v}{\partial z}, \frac{\partial w}{\partial x}, \frac{\partial w}{\partial y}, \frac{\partial w}{\partial z}\right). \quad (3)$$

The minimization step depends on the initial starting point of this vector, $\mathbf{w}_{3D,0}$. First, to improve the convergence behavior, only translation is taken into account. As a result, the partial derivatives in Eqs. (2a), (2b) and (3) vanish, and simple convolution remains. The location of the peak of the simplified function corresponds to the estimated displacement components u_0, v_0 and w_0 in whole voxels. Then, the Broyden–Fletcher–Goldfarb–Shanno (BFGS) algorithm, a quasi-Newton method (Press et al., 1994), is started with

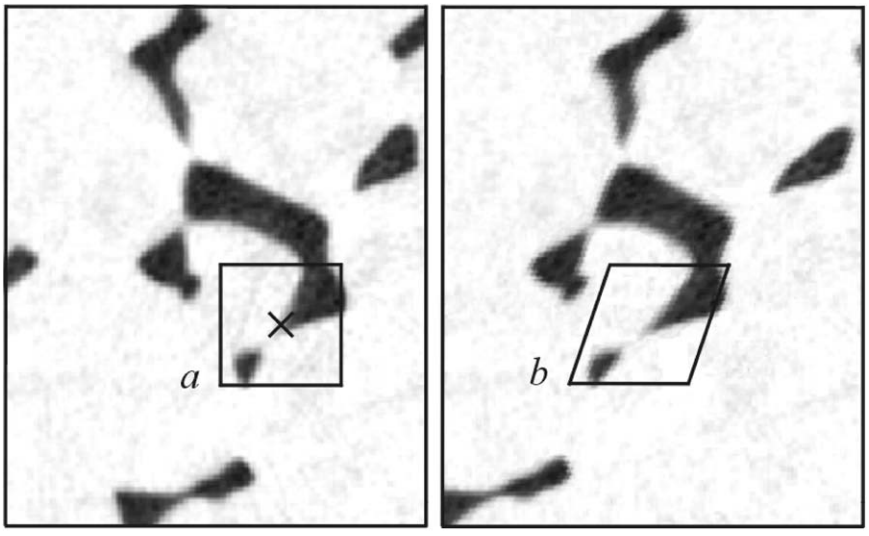

Fig. 1. Two-dimensional 36 μm CT-slice (inverted) of a 6101-T6 open-cell aluminum foam sample. The matrices a and b are used to calculated the displacement in the center of matrix a (indicated by the cross). They are schematically drawn in the reference (left) and an artificially deformed image (right).

$\mathbf{w}_{3D,0} = (u_0, v_0, w_0, 0, 0, 0, 0, 0, 0, 0, 0, 0)$. Four-point cubic interpolation with continuous second derivatives (Lehmann et al., 1999) is used to evaluate image values between adjacent voxels to enable displacement calculations with sub-voxel accuracy.

The displacement is only ascribed to the center of subset *a*. This subset is filled with voxel values or, through interpolation, with intermediate values at the sub-voxel level. This means that the displacement can be calculated anywhere in the reference image, provided that subsets *a* and *b* fit entirely in the images. In the two-dimensional case a uniform rectangular grid of points is often selected in the reference image, and displacements are calculated in each grid point. However, if the reference image represents a volume that is partially filled with a porous material, grid points are not necessarily located at the surface (where the strains are highest) and a certain amount of the grid points can be placed in the space between the trabeculae, as well. To create a suitable distribution of points in the solid structure and simultaneously enable easy visualization of the three-dimensional results, the meshing technique described in Frey et al. (1994) is used. It is based on the marching-cubes algorithm (Lorensen and Cline, 1987) that creates an iso-density surface. The method developed by Frey et al. fills the volume that is enclosed by the iso-density surface, with tetrahedrae, creating a volumetric FE-mesh. The displacement can now be calculated in each node with the three-dimensional digital image correlation technique. A three-dimensional mesh with displacement data is the result.

2.2. Strain calculation and visualization

Due to noise, a limited resolution of the images and a finite numerical precision in the minimization procedure, errors will occur in the displacement components calculated. Several methods are known to directly smooth the displacement data (Sutton et al., 1991) and convert this data to strains. However, a large portion of the nodes is located at the surface of the trabeculae, which complicates the smoothing procedure. Instead of filtering the displacement data, the deformation tensor $\mathbf{F} = \partial\mathbf{x}/\partial\mathbf{X}$ was determined from the unfiltered data. The tensor, which relates a vector $\mathbf{dx}$ in the deformed image with a vector $\mathbf{dX}$ in the reference image, is estimated in each element center with a least-squares fit through a certain amount of displacement data (Peters, 1987). The distance from the surrounding nodes to the element center, the so-called estimation radius, determines the amount of data that is taken into account. With a deformation tensor calculated in each element, the tetrahedron mesh is rebuilt. A single first node is fixed, and one-by-one each tetrahedron is added according to the estimated deformation tensor $\hat{\mathbf{F}}$. This tensor and the unit tensor $\mathbf{I}$ are used to compute the Green-Lagrange strain tensor $\hat{\mathbf{e}} = \frac{1}{2}(\hat{\mathbf{F}}^{C} \cdot \hat{\mathbf{F}} - \mathbf{I})$ in each element. The deformation and strains can be easily visualized with an arbitrary finite element post-processing tool. Here Mentat (MSC.Software Corporation, Santa Ana, US) was used to visualize the original and deformed FE-meshes. The original and deformed structures were also rendered with μCT Ray (V3.0, Scanco Medical, Basserdorf, CH). This enabled a qualitative validation of the image correlation technique.

2.3. Material and image acquisition

A Duocel open-cell aluminum foam (ERG Materials and Aerospace Corp., Oakland, US), with a trabecular bone like architecture was used as test material in this study. Two cubic samples, with an edge length of approximately 5 mm, a volume density of 0.07 and mean trabecular thickness of 0.3 mm, were sectioned from a larger piece of foam using a circular diamond saw.

Complete three-dimensional reconstructions of these samples were obtained by stacking sequential images created with a μCT device. In this study, two different devices were used, a Scanco μCT-80 (Scanco Medical, Bassersdorf, CH) for the first specimen and a Scanco μCT-40 for the second specimen. In all cases, the noise in the images was reduced with a three-dimensional Gauss-filter. A finite kernel size of 3 voxels and a function width (σ) of 0.6 voxels were chosen. Surface relaxation was applied to all the meshes based on the position of the nodes in the surrounding polygons (Perzl, 1997).

Because minimizing the function S (Eq. (1)) in three dimensions is time-consuming (with a subset size equal to $17 \times 17 \times 17$ voxels, analyzing the displacement in a single node required approximately 40 s on an 800 MHz personal computer), further analyses concentrated on a single trabecula near the surface of each specimen. This particular trabecula is clearly, but moderately deformed, which ensures a successful correlation and enables a visual validation. The first sample and its selected trabecula are shown in Fig. 2a. A similar trabecula was selected for the second specimen.

2.4. Accuracy and sensitivity study

To the authors' best knowledge, full three-dimensional digital image correlation techniques for strain measurements, as described in Section 2.1, were not reported in the literature. Therefore, several studies were done in order to establish the accuracy and sensitivity of the method. The applied settings for these studies are summarized in Table 1.

In a first study, the first specimen was scanned two times in the μCT-80 device at an isotropic spatial resolution of 36 μm. This resulted in two identical images of which the first image was used as a reference

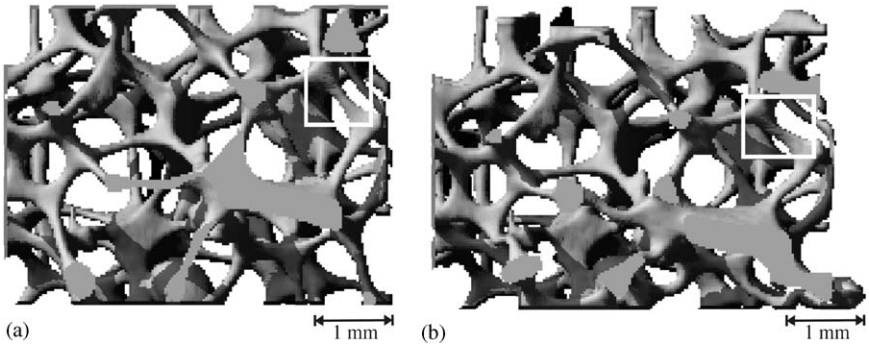

Fig. 2. Rendered parts of the first aluminum foam sample before (a) and after (b) the applied deformation. Three-dimensional digital image correlation is applied to the trabecula in the white box.

Table 1
Summary of the study settings. Correlated CT-scan pairs are enclosed by square brackets.

Study	Specimen nr.	Compressed or rotated	Resolution (μm)	Edge length (μm)	Subset size (μm) or (#voxels)	Estimation radius (μm) or (#voxels)	CT-scans
1	1	—	36	72	252, 468, 750 μm	72, 108, 144 μm	[1, 2]
2	1	R	36	72	468 μm	90 μm	[1, 3]
3	1	—	36	36, 72, 108	468 μm	144 μm, 4 voxels	[1, 2]
4	2	—	12, 20, 36	72	252 μm, 7 voxels	[a]	[4, 5] [6, 7] [8,9]
5	1	C	36	72	612 μm	90 μm	[1, 10]

[a] Strain calculations were not performed

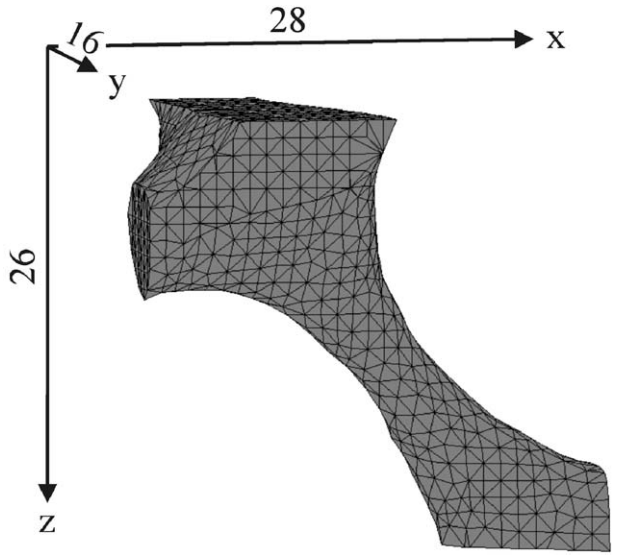

Fig. 3. Mesh representation of the selected trabecula. The solid part in a sub-volume of $28 \times 16 \times 26$ voxels was filled with tetrahedral elements. Interior and surface (except for the cutting edges) relaxation was applied to the mesh that consists of 5752 elements and 2130 nodes.

image. The selected trabecula was meshed with tetrahedral elements as described above. A cube edge length (Frey et al., 1994) of 72 μm was used, which resulted in a mesh representation of this selected trabecula with 5752 elements and 2130 nodes (Fig. 3) for the reference image. Since both images were obtained for the same specimen positioned in the same way, the correlation procedure should results in the calculation of a zero displacement and strain fields. In this first study, the subset size N was set to 7, 13 and 21 voxels to study the effect of this parameter on the calculated displacement field. The displacements obtained were subsequently converted to strains using estimation radii of 72, 108 and 144 μm to study the effect of the estimation radius on the calculated strain field for each of the chosen subset dimensions.

In a second study, the influence of a combined rigid translation/rotation on the calculated displacement and strain fields for the selected trabecula was determined. The sample was rotated about the vertical axis by approximately 8.5° and scanned a third time in the μCT-80 device at the same resolution of 36 μm. Displacements were calculated for the 2130 nodes using a subset size of $13 \times 13 \times 13$ voxels, corresponding to 468 μm. The distributions of the strain components in the original and rotated situations were calculated using an estimation radius of 90 μm.

In a third study, two additional meshes were created to study the influence of the tetrahedron size on the calculated strain field. Cube edge lengths of 36 and 108 μm resulted in meshes with 25486 and 2454 elements and 9459 and 917 nodes, respectively, for the selected trabecula. The estimation radius was first held at a constant size of 144 μm and later adjusted in such a way that the number of nodes in the estimation volume was held constant at 47.

In a fourth study, the influence of spatial resolution was studied. Using the second sample, two sets of images were created at a resolution of 12, 20 and 36 μm using the μCT-40 scanner in a similar way as done for the first sample. A cube edge length of 72 μm resulted in meshes consisting of 1541, 1503 and 1452 nodes and 5804, 5647 and 5368 elements for the reference images with spatial resolutions of 12, 20 and 36 μm, respectively. To determine the influence of spatial resolution alone, the physical size of the subset region was first held constant at a size of about 255 μm. This resulted in subset sizes of $7\times7\times7$, $13\times13\times13$ and $21\times21\times21$ voxels for the 36 μm, 20 μm and 12 μm resolution images, respectively. Following, the subset region was held constant at a dimension of $7\times7\times7$ voxels.

In a final study, the first sample was loaded to a continuum-level strain value of 0.2 and then unloaded, after which it was scanned a last time using the μCT-80 device at a resolution of 36 μm. A subset size of $17\times17\times17$ voxels was used to calculate the displacement in the tetrahedron nodes (Fig. 3). An estimation radius of 90 μm, approximately one half of the minimal width of the selected trabecula, was chosen for the strain calculation. The mesh is deformed according to the estimated strain tensors in the tetrahedral elements.

3. Results

The displacements (mean ± standard deviation) obtained from the first study are shown in Fig. 4. These results show that an offset of almost 10 μm in the z-direction exists between the first and the repeated measurement. Because the sample was not removed from the device between the creations of the two images, this offset must be caused by the finite positioning precision of the μCT device. This offset-displacement does not affect the strain measurements. The strain results presented in Fig. 5, however, show that the zz-component of the Green-Lagrange strain has a larger variance than the other components, which means that there is also a random error in the vertical positioning when scanning sequential slices. Although this random positioning error is small (less than a micron), it directly affects the accuracy of the strain calculation in the z-direction. Fig. 5 also shows that a rigid translation and rotation, as was done for the third study, does not affect the precision of the strain calculation. Very similar histograms were found for the specimen in the original and rotated positions.

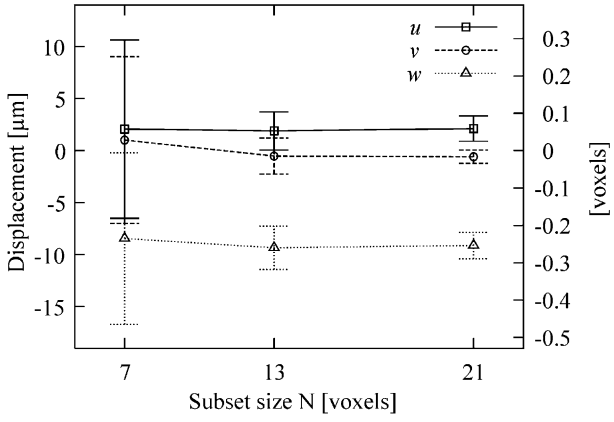

Fig. 4. Calculated displacement components u, v and w in μm and voxels as a function of the subset size (error bars represent one standard deviation).

The mean of the six strain components for the first study is shown in Fig. 6 as a function of the subset size. Doubling the subset size N resulted in a standard deviation of approximately 30% of the original value. The estimation radius had a large effect on the standard deviation of the strain distribution as well. Estimation radii of 72, 108 and 144 μm led to a deformation tensor in each element center that is estimated from the displacement data in 24.7 ± 3.0, 60.8 ± 7.3 or 113.7 ± 15.0 nodes, respectively. Doubling the amount of nodes in the estimation volume decreased the standard deviation by roughly 35%.

When the edge length is varied, as done in the third study, while holding the estimation radius at a constant size (in μm), more nodes are used to estimate the strain

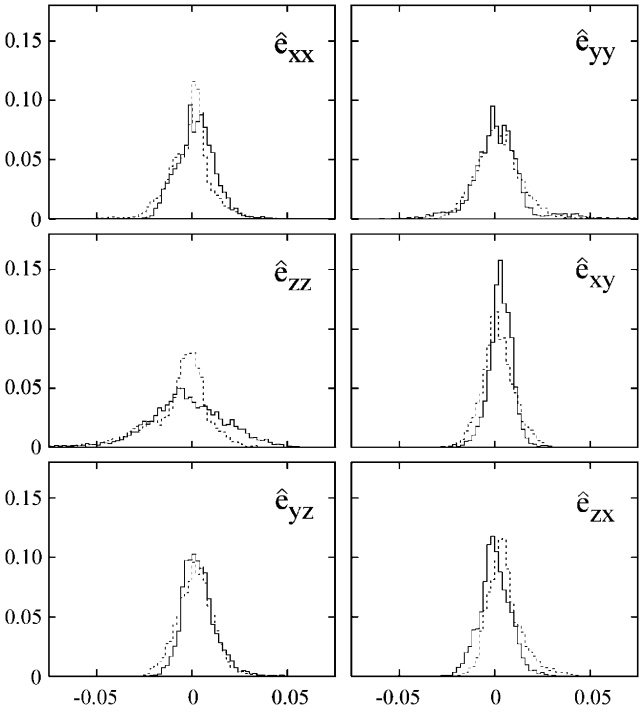

Fig. 5. Histograms of the Green-Lagrange strain components in the 5752 elements. A subset of $17\times17\times17$ voxels and an estimation radius of 72 μm were used. Similar distributions are found for both the baseline test (solid line) and rotation test (dotted line). The horizontal and vertical axes represent the strain [-] and fraction in each bin [-], respectively.

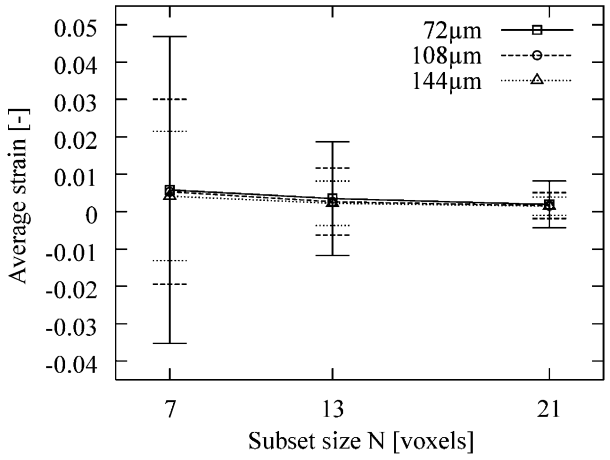

Fig. 6. Average of the six components of the Green-Lagrange strain tensor as a function of the subset size. Estimation radii of 72, 108 and 144 µm were used to estimate the deformation tensor.

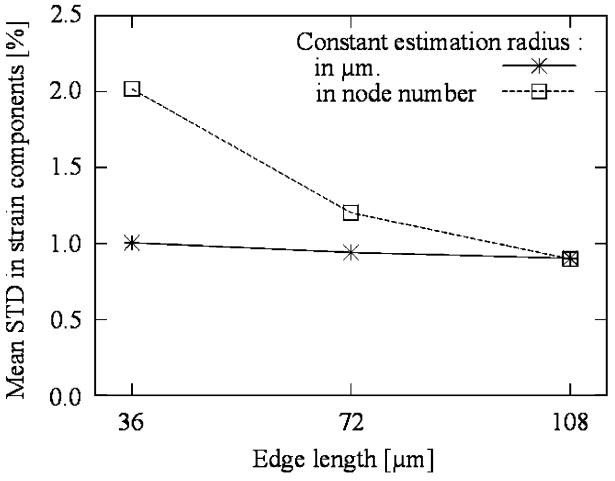

Fig. 7. Effect of variations in the image resolution at a fixed subset size (in micrometers or voxels). The standard deviation (STD) is calculated for the three displacement components and then averaged. The open boxes represent a subset of $7\times7\times7$ voxels. The crosses represent a subset size of 252 µm (i.e. $7\times7\times7$, $13\times13\times13$ and $21\times21\times21$ voxels for the 36, 20 and 12 µm images, respectively).

components. The results for the third test (Fig. 7) show that the use of more nodes did not affect the precision. When the number of nodes was held constant, however, the standard deviation increased with increasing edge length.

The influence of image resolution on the standard deviation in the average displacement, tested in the fourth study, is shown in Fig. 8. When the physical dimension of the subset was held constant, the standard deviation changed less than a micrometer with increasing resolution. However, the precision of the calculated displacement field deteriorated when the number of voxels in the subset size was held constant, although the correlation was based on the same amount of data.

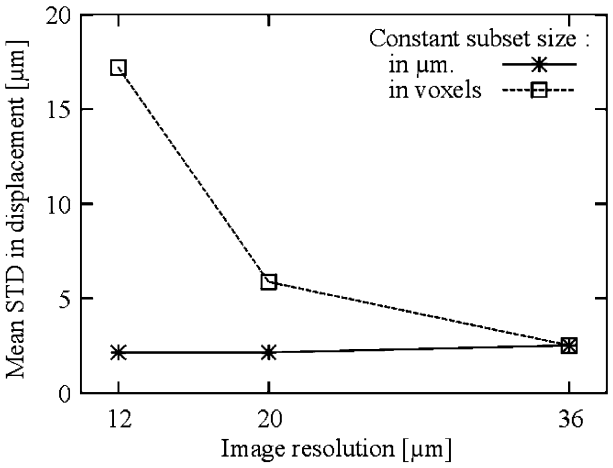

Fig. 8. Effect of variations in the edge length for a fixed estimation volume (in micrometers or node number). The standard deviation (STD) is calculated for the six strain components and then averaged. The open boxes represent the average strain estimated from 47 nodes (estimation radii of 49.7 ± 2.0, 96.7 ± 5.1 and 144.1 ± 9.2 µm). The crosses represent an estimation radius of 144 µm.

The shape of the selected trabecula, in rendered and mesh representation, before and after the applied deformation, is presented in Fig. 9. The deformed mesh was obtained by applying the estimated deformation to the original mesh. The calculated equivalent Green-Lagrange strain is shown in the deformed meshes.

4. Discussion

This article presents a three-dimensional digital image correlation technique that uses CT-images of open-cell structures for strain measurements in single trabeculae. Three-dimensional digital image correlation has been used earlier for strain measurements in trabecular bone samples by Bay et al. (1999). However, only homogenized strains were calculated with their technique, which neglects the deformation of the subset. For better understanding the deformations of trabecular bone or trabecular tissue, local strains are needed. The method presented uses tetrahedronization (Frey et al., 1994) and linear deformation of the subset (Sutton et al., 1983) to enable the calculation and visualization of local strains in single trabeculae.

The CT-images of the aluminum alloy showed little variation in gray-values within the structure compared to the speckle images (e.g. Sutton et al., 1983), trabecular texture images (e.g. Bay, 1995) and cortical bone images (e.g. Nicolella et al., 2001). This means that the correlation procedure is mainly based on the surface of the rods. Nevertheless, a reasonable precision can be achieved for the displacement components compared to the expected precision in two (Sutton et al., 1986) and three dimensions (Bay et al., 1999). In the present study,

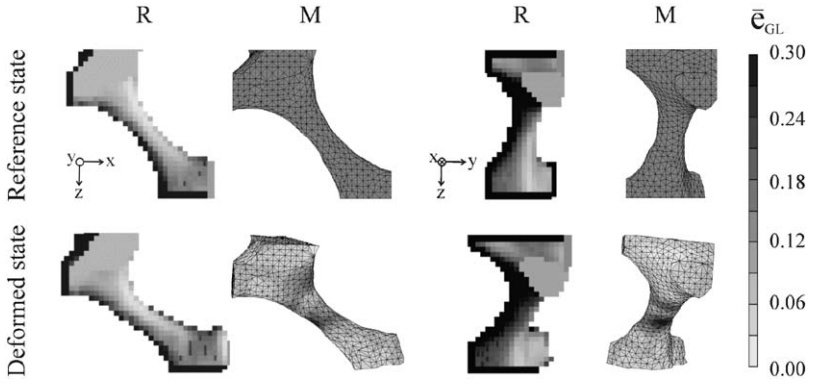

Fig. 9. Comparison between the calculated deformation and the rendered 36 μm CT-scan images (R = rendered image, M = mesh). The equivalent Green-Lagrange strain $\bar{e}_{GL} = \sqrt{\frac{2}{3}\hat{\mathbf{e}} : \hat{\mathbf{e}}}$ is shown in the deformed FE-meshes. The deformation tensor is estimated in each element center from the surrounding displacement data in a sphere with a radius of 90 μm (39.9 ± 4.8 nodes). The deformed mesh is obtained by applying each deformation tensor to the accompanying tetrahedral element.

trabecular bone was replaced with an open-cell aluminum foam sample with a structure similar to low-density trabecular bone. In general, the aluminum rods are, however, thicker than the trabeculae in real trabecular bone (50–250 μm, Mullender et al., 1996). In addition, the structure of the aluminum foam is predominantly rod-like, where trabecular bone can be plate-like as well. Although CT-images of trabecular bone might reveal more information about the internal structure, it is not known if the accuracy is improved when trabecular bone is analyzed with the image correlation technique instead of aluminum foam.

Local strains in trabeculae in situ can be quantified with the three-dimensional digital image correlation technique. Typical values for the standard deviation in the displacement and strain components are 2.0 μm and 0.01, respectively. These values are based on the precision tests involving undeformed samples. When dealing with deformed samples, the precision is likely to decrease due to complex (non-linear) deformation patterns. Nonetheless, visual agreement exists between the rendered images and the, through the estimated deformation, deformed meshes. Rigid translations do not cause any problems, as long as the images contain the structure before and after the translation. However, it is not known to what extent rotations and deformations can be accurately estimated.

The standard deviations in the estimated strain limit the technique to strain measurements beyond the yield point of bone tissue (based on bovine cortical bone tissue (Burstein et al., 1975)). This might be a problem when certain biological and mechanical processes are studied. However, this technique can be used to determine the local strains, which can exceed 20% (Yeh et al., 2001; Dannemann and Lankford, 2000), in experimentally deformed single trabeculae (Yeh et al., 2001) or to validate the non-linear finite element models that are used to simulate failure of trabecular bone (Niebur et al., 2000) and aluminum foam structures (Verhulp et al., 2003). The precision can be increased by increasing (1) the subset size, (2) the finite element size or (3) the estimation radius. However, this also decreases the resolution in the strain map. From pilot studies it was concluded that four-point cubic interpolation (Lehmann et al., 1999) and a linear method for the deformation tensor estimation (Peters, 1987) were both fast and accurate. Using six-point cubic interpolation (Lehmann et al., 1999) and/or a higher order estimation method (Geers et al., 1996) did not have a significant effect on the precision. However, a higher resolution in the computed tomography images or other scanning methods such as synchrotron radiation could be an answer. Increasing the resolution might reveal the distinct casting features on the surface of the aluminum alloy (Nieh et al., 2000; Zhou et al., 2002). In case of trabecular bone, the heterogeneous internal structure of the trabecular bone tissue (Choi and Goldstein, 1992) could become visible. In that case the procedure is not only based on the surface of the rods and should, therefore, enable a more accurate strain measurement.

Acknowledgements

The authors wish to acknowledge the technical support of Prof. Marc G.D. Geers. We also thank Prof. Ralph Müller from the Institute of Biomedical Engineering of the ETH/University Zurich for the use of their μCT-40 device and his help in this project.

References

Bay, B.K., 1995. Texture correlation: a method for the measurement of detailed strain distributions within trabecular bone. Journal of Orthopaedic Research 13 (2), 258–267.

Bay, B.K., Smith, T.S., Fyhrie, D.P., Saad, M., 1999. Digital volume correlation: three-dimensional strain mapping using X-ray tomography. Experimental Mechanics 39 (3), 217–226.

Burstein, A.H., Zika, J.M., Heiple, K.G., Klein, L., 1975. Contribution of collagen and mineral to the elastic–plastic properties of bone. Journal of bone and joint surgery A 57 (7), 956–961.

Choi, K., Goldstein, S.A., 1992. A comparison of the fatigue behavior of human trabecular and cortical bone tissue. Journal of Biomechanics 25 (12), 1371–1381.

Dannemann, K.A., Lankford Jr., J., 2000. High strain rate compression of closed-cell aluminum foams. Materials Science and Engineering A293, 157–164.

Frey, P., Sarter, B., Gautherie, M., 1994. Fully automatic mesh generation for 3-D domains based upon voxel sets. International Journal for Numerical Methods in Engineering 37 (16), 2735–2753.

Geers, M.G.D., De Borst, R., Brekelmans, W.A.M., 1996. Computing strain fields from discrete displacement fields in 2D-solids. International Journal of Solids and Structures 33 (29), 4293–4307.

Hollister, S.J., Brennan, J.M., Kikuchi, N., 1994. A homogenization sampling procedure for calculating trabecular bone effective stiffness and tissue level stress. Journal of Biomechanics 27 (4), 433–444.

Lehmann, T.M., Gönner, C., Spitzer, K., 1999. Survey: interpolation methods in medical image processing. IEEE Transactions on Medical Imaging 18 (11), 1049–1075.

Lorensen, W.E., Cline, H.E., 1987. Marching cubes: a high resolution 3D surface construction algorithm. Computer Graphics 21 (4), 163–169.

Mullender, M.G., Huiskes, R., Versleyen, H., Buma, P., 1996. Osteocyte density and histomorphometric parameters in cancellous bone of the proximal femur in five mammalian species. Journal of Orthopaedic Research 14 (6), 972–979.

Nicolella, D.P., Nicholls, A.E., Lankford, J., Davy, D.T., 2001. Machine vision photogrammetry: a technique for measurement of microstructural strain in cortical bone. Journal of Biomechanics 34 (1), 135–139.

Niebur, G.L., Feldstein, M.J., Yuen, J.C., Chen T, J., Keaveny, T.M., 2000. High-resolution finite element models with tissue strength asymmetry accurately predict failure of trabecular bone. Journal of Biomechanics 33 (12), 1575–1583.

Nieh, T.G., Higashi, K., Wadsworth, J., 2000. Effect of cell morphology on the compressive properties of open-cell aluminum foams. Materials Science and Engineering A 283, 105–110.

Odgaard, A., Linde, F., 1991. The underestimation of young's modulus in compressive testing of cancellous bone specimens. Journal of Biomechanics 24 (8), 691–698.

Perzl, M.A., 1997. Development of 3D models for the simulation of fluid dynamics and particle transport in realistic airway geometries. Ph.D. Thesis, Faculty of Mathematics, Munich University of Technology.

Peters, G., 1987. Tools for the measurement of stress and strain fields in soft tissue. Ph.D. Thesis, Eindhoven University of Technology.

Press, W.H., Teukolsky, S.A., Vetterling, W.T., Flannery, B.P., 1994. Numerical Recipes in Fortran 77: the art of scientific computing. Cambridge University Press, Cambridge.

Sutton, M.A., Wolters, W.J., Peters, W.H., Ranson, W.F., McNeill, S.R., 1983. Determination of displacements using an improved digital correlation method. Image and Vision Computing 1 (3), 133–139.

Sutton, M.A., Cheng, M., Peters, W.H., Chao, Y.J., McNeill, S.R., 1986. Application of an optimized digital correlation method to planar deformation analysis. Image and Vision Computing 4 (3), 143–150.

Sutton, M.A., Turner, J.L., Bruck, H.A., Chae, T.A., 1991. Full-field representation of discretely sampled surface deformation for displacement and strain analysis. Experimental Mechanics 31, 168–177.

van Rietbergen, B., Weinans, H., Huiskes, R., Odgaard, A., 1995. A new method to determine trabecular bone elastic properties and loading using micromechanical finite-element models. Journal of Biomechanics 28 (1), 69–81.

van Rietbergen, B., Müller, R., Ulrich, D., Rüegsegger, P., Huiskes, R., 1999. Tissue stresses and strain in trabeculae of a canine proximal femur can be quantified from computer reconstructions. Journal of Biomechanics 32 (2), 165–173.

Verhulp, E., van Rietbergen, B., Müller, R., Huiskes, R., 2003. Simulation of the failure behavior of trabecular bone-like structures. In: Proceedings of the 5th International Symposium on Computer Methods in Biomechanics & Biomedical Engineering, Rome, Italy.

Yeh, O.C., Keaveny, T.M., Tischner, T.T., 2001. Fracture strains of trabecular tissue exceed 20% in bending. poster 520, 47th Annual Meeting, Orthopaedic Research Society, San Francisco, CA.

Zhou, J., Mercer, C., Soboyejo, W.O., 2002. An investigation of the microstructure and strength of open-cell 6101 aluminum foams. Metallurgical and Materials Transactions A 33 (5), 1413–1427.